Resolving the two-dimensional ANNNI model using transfer matrices

Yi Hu[1] and Patrick Charbonneau[1,2,*]

[1] *Department of Chemistry, Duke University, Durham, North Carolina 27708, USA*
[2] *Department of Physics, Duke University, Durham, North Carolina 27708, USA*

(Dated: March 15, 2021)

Some features of the phase diagram of the two-dimensional ANNNI model have long been debated. The extended structural correlations and relaxation times associated with its Kosterlitz-Thouless (KT) phase indeed result in analytical and numerical treatments making contradictory predictions. Here, we introduce a numerical transfer matrix approach that bypasses these problems, and thus clears up various ambiguities. In particular, we confirm the transition temperatures and the order of the transition to the floating incommensurate phase. Our approach motivates considering transfer matrices for solving long-standing problems in related models.

Introduction. Patterned and modulated phases robustly form when the components of a system interact via competing short-range attractive and long-range repulsive (SALR) interactions.[1–4] Such phases have indeed been observed in materials as varied as magnetic alloys,[5,6] semiconducting nanowires,[7] lipidic surfactants[8,9] and biological tissues.[10,11] Frustration, however, is also associated with slowly decaying finite-size corrections and complex relaxation processes, which both severely impede the study of equilibrium phases. In numerical simulations, for instance, specialized sampling techniques are needed to study even minimal microphase formers,[12–16] let along more realistic ones.

Lattice archetypes with SALR interactions were first formulated forty years ago, the simplest being the axial next-nearest-neighbor Ising (ANNNI) model.[17] Yet even in two dimensions this small perturbation of the simple Ising case is out of reach of exact treatments. Different approximation methods have thus been considered, including the Hamiltonian limit,[18–20] the free fermion approximation,[21] high-temperature series expansion,[22] and others.[23–26] These approaches, however, do not always concur. For instance, the cluster variational method (CVM) gives a fairly wide range of incommensurate (IC) phase[23] while a density variation renormalization group (DMRG) study[26] suggests the IC phase only exists over an infinitesimal temperature range. As a result, although the physics of both the small frustration regime and the energetic ground states has long been solved, that of the finite temperature-strong frustration regime has not. Between the standard high-temperature paramagnetic phase and low-temperature modulated antiphase, a floating IC phase likely intercalates. A field-theoretic treatment suggests that this critical phase—if it exists—is of the Kosterlitz-Thouless (KT) type, and thus belongs to the XY universality class.[27,28] Numerical validation, however, has remained elusive, as has whether the IC phase persists at large frustrations or disappears at a Lifshitz point.[25] Equibrium Monte Carlo simulation approaches have reported different high and low transition temperatures,[14,29–31] T_{c1} and T_{c2}, respectively. (Non-equilibrium relaxation simulations suggesting that the IC phase has but an infinitesimal width[32,33] have since been refuted.[14]) The proposed reentrance of the IC phase around the multiphase point[23,24] also remains to be confirmed. Because these features are central to our understanding of the floating IC phase in microphase formers, clarifying their nature is particularly important.

As was recognized already in the mid-1980s, a transfer-matrix (TM) approach should be able to sort out these issues.[34,35] For semi-infinite systems, the approach provides exact solutions that can then be extrapolated to the thermodynamic limit by careful scaling. Because both computational and space complexity grow exponentially with system size, however, the accessible size range has long been too narrow for physical insight to emerge from TM studies. Thanks to marked improvements in methodology, computer hardware and eigensolvers,[36] the TM approach has recently been applied to more complex (quasi) one-dimensional continuum-space systems, including SALR models with up to third-nearest-neighbor interactions,[37] and hard spheres in cylindrical confinement up to next-nearest-neighbor interactions.[38–40] For two-dimensional lattice models with frustration, sufficiently large systems have also recently become accessible to the TM approach, thus enabling transition temperatures on the related $J_1 - J_2$ model to be determined.[41] In this Letter, we push the effective use of the TM formalism to resolve various physical ambiguities of the somewhat more complex ANNNI model. In particular, we determine the phase boundaries for the floating IC phase, and critically assess proposals for the Lifshitz point and the IC phase reentrance.

Transfer matrix approach. The ANNNI model Hamiltonian for Ising spin variables, $s_i = \pm 1$, reads

$$\mathcal{H}_{\text{ANNNI}} = -J_1 \sum_{\langle i,j \rangle} s_i s_j + J_2 \sum_{[i,j]_{\text{axial}}} s_i s_j - J_0 \sum_i s_i, \quad (1)$$

where the coupling constant $J = J_1 > 0$ sets the scale for the frustration along the axial next-nearest-neighbor direction $\kappa = J_2/J_1 > 0$ and the external field $h = J_0/J$. For $\kappa = 0$, the model reduces to the standard Ising model; for the $T = 0$ ground state, ferromagnetic order dominates until $\kappa < 1/2$, and the periodic antiphase (with periodicity $\langle 2 \rangle$) takes overs for $\kappa > 1/2$. Because in lattice-

gas representation, $n_i = (s_i + 1)/2$, the ANNNI model corresponds to SALR interacting particles with effective chemical potential h, it is also a minimal description of layered microphases.

The finite-temperature, finite-frustration phase behavior of semi-infinite strips is obtained by a TM approach with each layer $\mathbf{s}$ having L spins $s_1, s_2, ..., s_L$. (Setting $s_{L+1} \equiv s_1$ imposes periodic boundary conditions.) Because the interaction in the ANNNI model is anisotropic, the TM can be propagated either perpendicular ($_\perp$TM)[34] or parallel ($_\parallel$TM)[35] to the axial next-nearest-neighbor interaction direction. In both cases, the matrices can be decomposed into intra-layer, $\mathbf{T}_x$, and inter-layer, $\mathbf{T}_y$, contributions,

$$\mathbf{T} = \mathbf{T}_x^{\frac{1}{2}} \mathbf{T}_y \mathbf{T}_x^{\frac{1}{2}}. \tag{2}$$

In $_\perp$TM, row and column indices correspond to neighboring layer configurations $\mathbf{s}$ and $\mathbf{s}'$,

$$\begin{cases} {}_\perp\mathbf{T}_x(\mathbf{s}) & = \exp\Big[J\sum_{i=1}^{L}(s_i s_{i+1} - \kappa s_i s_{i+2} + h s_i)\Big], \\ {}_\perp\mathbf{T}_y(\mathbf{s},\mathbf{s}') & = \exp\Big(J\sum_{i=1}^{L} s_i s_i'\Big), \end{cases} \tag{3}$$

which makes $_\perp\mathbf{T}$ a $2^L \times 2^L$ symmetric dense matrix. In $_\parallel$TM, row and column indices correspond to two subsequent layers $\{\mathbf{s},\mathbf{s}'\}$ and $\{\mathbf{s}',\mathbf{s}''\}$, respectively, and then

$$\begin{cases} {}_\parallel\mathbf{T}_x(\mathbf{s},\mathbf{s}') & = \exp\Big[J\sum_{i=1}^{L}(s_i s_{i+1} + s_i s_i' + h s_i)\Big], \\ {}_\parallel\mathbf{T}_y(\mathbf{s},\mathbf{s}'') & = \exp\Big(-\kappa J\sum_{i=1}^{L} s_i s_i''\Big), \end{cases} \tag{4}$$

which makes $_\parallel\mathbf{T}$ a $4^L \times 4^L$ non-symmetric sparse matrix with 8^L nonzero entries.

The leading eigenvalue (that with the largest magnitude) of these matrices, λ_0, provides the free energy per spin, $f = -\log\lambda_0/(\beta L)$, and the product of left and right leading eigenvectors, $P(\mathbf{s}) = \varphi^{-1}(\mathbf{s})\varphi(\mathbf{s})$, provides the equilibrium probability of a layer configuration. Equilibrium configurations can thus be efficiently planted.[42] Taking partial derivatives of f provides thermal properties, such as the energy $u = -k_B T^2 \partial(\beta f)/\partial T$ and specific heat $c = \partial u/\partial T$ per spin. The leading correlation length can also be obtained from the spectrum gap, $\xi_1 = 1/\log(\lambda_0/|\lambda_1|)$,[35] albeit only along the direction of layer propagation. Hence, although the compactness of $_\perp$TM brings larger L within computational reach, the $_\parallel$TM geometry is more informative about the modulation structure.

Iterative eigensolvers based on matrix-vector multiplication are used to obtain first a few leading eigenvalues and eigenvectors.[43] When only the leading eigenpairs is needed, the eigenproblem can be solved equivalently on a reduced transfer matrix,[34] knowing that the original matrix is invariant to re-indexing by shifting one spin or counting spins backwards, and has Z_2 symmetry when $h = 0$. Combining these equivalent configurations generically reduces the matrix size by a factor of $2L$ ($4L$ when $h = 0$). As a result, $_\perp$TM systems with up to $L = 36$ and $_\parallel$TM systems with up to $L = 16$ can be efficiently solved using < 60GB of memory.

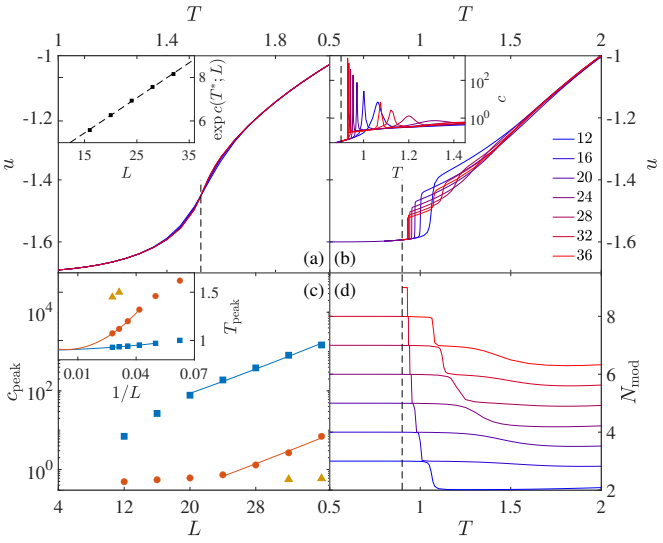

FIG. 1. Thermodynamic and structural observables from $_\perp$TM. Evolution of the energy for (a) $\kappa = 0.3$ and (b) 0.6 with corresponding phase transition temperature estimates, T_c and T_{c2}, respectively (dashed lines). (insets) For the former, the heat capacity peak, $c(T^*;L)$, grows logarithmically with system size; for the latter, the heat capacity curves present distinct peaks that sharpen with L. For $\kappa = 0.6$: (c) the peak height of the lowest temperature peak, $c(T^*;L)$, grows exponentially with system size. (Inset) Extrapolating T^* with a quadratic form in $1/L$ suggests $T_{c2} = 0.90(1)$, and the second peak is projected to merge with the first as $1/L \to 0$. (d) The number of modulation blocks on a layer N_{mod} correspondingly decreases stepwise with T.

Phase diagram for $h = 0$. We first consider results from the $_\perp$TM route in absence of an external field (Fig. 1). For $\kappa < 1/2$, energy curves for different L robustly cross at a well-defined critical point $T_c(\kappa)$. For the Ising, $\kappa = 0$, limit $u(T_c)$ is perfectly invariant with L,[44,45] and for $0 < \kappa \lesssim 1/2$, small systems with $L \lesssim 10$ exhibit a correction of at most 0.1%. From this identification of $T_c(\kappa)$ we confirm that the heat capacity peak, $c(T^*;L)$, grows logarithmically with system size in this regime (Fig. 1(a) inset), as expected for systems in the Ising universality class.

For $\kappa \gtrsim 1/2$ a markedly different behavior is observed. As in simulations,[30] $u(T)$ displays pronounced steps, thus giving rise to sharp heat capacity peaks (Fig. 1(b)). Extrapolating the lowest peak temperature for $\kappa = 0.6$ using a quadratic form in $1/L$ gives a thermodynamic limit, $1/L \to 0$, transition temperature consistent with recent numerics for T_{c2}.[31] At first glance, these sharp features suggest a standard first-order transition,[46,47] but the step height scales as $1/L$ (not shown), and is thus projected to vanish in the thermodynamic limit. Confusingly, the peak height of the specific heat nonetheless scales exponentially, $c(T^*;L) \sim \exp(aL)/L$ (up to $c \geq 10^3$)

(Fig. 1(c)), i.e., faster than any power-law. These observations are in fact reminiscent of the Pokrovsky-Talapov transition scenario.[48] In $d = 2$, this second-order transition is expected to have heat capacity exponents $\alpha = 1/2$ and $\alpha' \to \infty$ from the floating IC and commensurate $\langle 2 \rangle$ phases, respectively.[49] Although the first scaling has long been validated from the square-root singularity of the modulation wavenumber,[25,26,29] limited simulation accuracy prevented confirming the second.[30] The exponential growth of the heat capacity peak obtained by the TM formalism completes its characterization.

Observations in the vicinity of $T \geq T_{c2}$ further validate the nature of the IC phase. As L increases, multiple heat capacity peaks emerge, accompanied by a stepwise evolution of the energy u and by a quantization of the number of modulation layers, $N_{\rm mod}$ (Fig. 1(b, d)). The second heat capacity peak that emerges for $L \geq 24$ also grows exponentially with L, and is projected to merge with the first peak as $1/L \to 0$ (Fig. 1 (c) inset); a third peak similarly appears for $L \geq 32$. For $_\perp$TM, the modulation wavenumber $q = N_{\rm mod}/L$, also decreases stepwise with T and the step height scales as $1/L$. In other words, at finite L the allowed modulations are separated by sharp crossovers, but as $1/L \to 0$ infinite commensurate phases are separated by infinitesimal temperature intervals. Each of these steps can be viewed as a "phase transition" of infinitesimal singularity, a hallmark of the persistent criticality of the floating IC phase.

As temperature increases, the floating IC to paramagnetic phase transition at T_{c1} leaves no thermal signature, as expected of a KT-type transition. Certain observables used for identifying T_{c2}, such as the wavevector q and the domain free energy, thus exhibit no signature at T_{c1}.[26] To determine T_{c1}, we instead investigate the correlation length ξ_1 in $_\parallel$TM. Specifically, following the finite-size analysis proposed in Ref. 35, we define

$$Y_L = \frac{\log[\xi_1(L+1)] - \log[\xi_1(L-1)]}{\log(L+1) - \log(L-1)}, \qquad (5)$$

which is the finite-L (effective or local) critical exponent for ξ_1, i.e., $\xi_1 \sim L^{Y_L}$. Because the thermodynamic limit of this quantity gives the anisotropic scaling exponent, i.e., $\lim_{L\to\infty} Y_L = \theta$,[50] different thermodynamic scenarios can be discerned:

$$\begin{cases} \text{in the ordered phase,} & Y_L \to \infty, \\ \text{in the disordered phase,} & Y_L \to 0, \\ \text{in the critical phase, or at } T_c, & Y_L \to \text{cnst} > 0. \end{cases}$$

Reference 35 also proposed extracting the modulation wavenumber q directly from the angular argument of the subleading eigenvalue, i.e., $q = |\arg(\lambda_1)|/2\pi$. This quantity brings about another local exponent, Z_L, which characterizes the convergence to the ground state modulation,

$$Z_L = -\frac{\log[\delta q(L+1)] - \log[\delta q(L-1)]}{\log(L+1) - \log(L-1)}, \qquad (6)$$

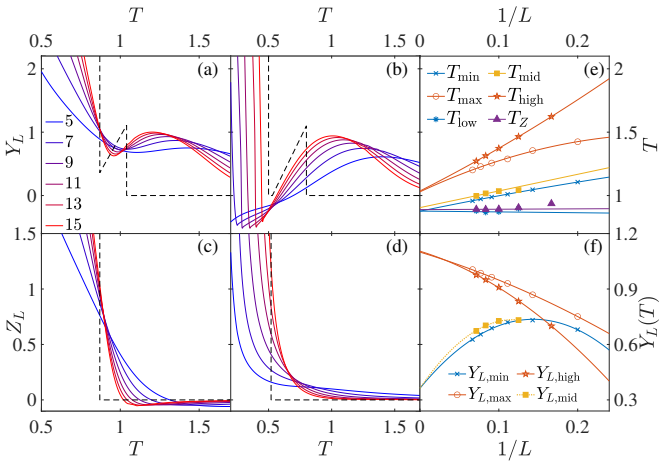

FIG. 2. Correlation length analysis from $_\parallel$TM. Local exponents (a, b) Y_L and (c, d) Z_L for $\kappa = 0.6$ and 0.49, respectively. For $\kappa = 0.6$: (e) the two characteristic temperatures extracted from Y_L and Z_L (see text for details) coincide at T_{c1} and T_{c2}, respectively, as $1/L \to 0$; (f) the critical exponents Y_L also coincide at these temperatures. In (e) and (f), solid lines are quadratic fits (or linear fits if only three data points are available). The dotted line in $Y_{L,\rm mid}$ is purely qualitative because of the limited number of available data points. The thermodynamic behavior of Y_L and Z_L, extracted from panels (e) and (f), are reported in (a-d) (dashed lines).

where $\delta q = |q - q(T = 0)|$, and similarly,

$$\begin{cases} \text{in the commensurate phase,} & Z_L \to \infty, \\ \text{in the IC phase,} & Z_L \to 0, \\ \text{at the IC transition or disorder line,} & Z_L \to \text{cnst} > 0. \end{cases}$$

Without loss of generality, we here consider results for $\kappa = 0.6$. Figure 2(a) shows the non-monotonic evolution of Y_L with T. Multiple crossing points ($T_{\rm low}$, $T_{\rm mid}$ and $T_{\rm high}$) as well as local extrema ($T_{\rm min}$ and $T_{\rm max}$) can then be identified, in addition to the crossing point in Z_L, denoted T_Z (Fig. 2(c)). The finite-L scaling of these characteristic temperatures numerically determines the transition temperatures as well as the corresponding θ (Fig. 2(e, f)). In Ref. 35 and 50, the floating IC phase could be loosely bound by T_Z and $T_{\rm high}$; here, thanks to a vastly larger range of L being accessible, more characteristic temperatures can be analyzed, thus refining numerical estimates and clarifying the underlying physics.

To extract thermodynamic information, we consider again a quadratic fit of these characteristic temperatures with $1/L$. Although this choice arbitrarily assumes a critical scaling of L^{-t} with $t = 1$—no theoretical estimate of t is known—it nevertheless leads to a good convergence of the characteristic temperatures in the thermodynamic limit. $T_{\rm low}, T_{\rm mid}$, $T_{\rm min}$ and T_Z all coincide to $T_{c2} = 0.89(1)$, consistent with the $_\perp$TM analysis, and $T_{\rm max}$ and $T_{\rm high}$ both coincide at $T_{c1} = 1.04(1) > T_{c2}$. This second temperature, however, markedly differs from the two most recent simulation estimates, $T = 1.16(1)$[14]

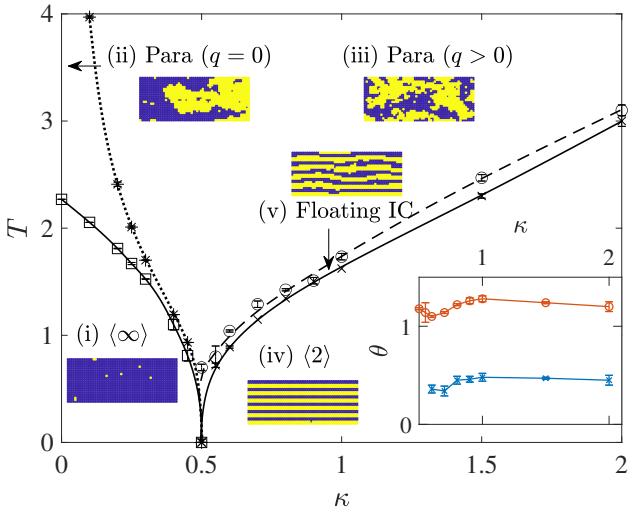

FIG. 3. Phase diagram for the two-dimensional ANNNI model with $h = 0$. The TM approach provides phase boundaries for the ferromagnetic $\langle\infty\rangle$-paramagnetic (squares), commensurate antiphase $\langle 2\rangle$-floating IC (crosses), and paramagnetic-floating IC (circles) transitions. The disorder line (asterisks) subdivides the paramagnetic phase in two regimes with $q = 0$ and $q > 0$ modulation wavevectors. Configuration snapshots generated by planting use blue and yellow pixels to denote $+1$ and -1 spins, respectively. (Inset) Extrapolated exponents at the boundaries of the floating IC phase, $\theta(T_{c1};\kappa)$ (orange) and $\theta(T_{c2};\kappa)$ (blue). Error bars denote the range of the extrapolated results obtained from different characteristic temperatures (see Fig. 2(f)). Lines are guides to the eyes.

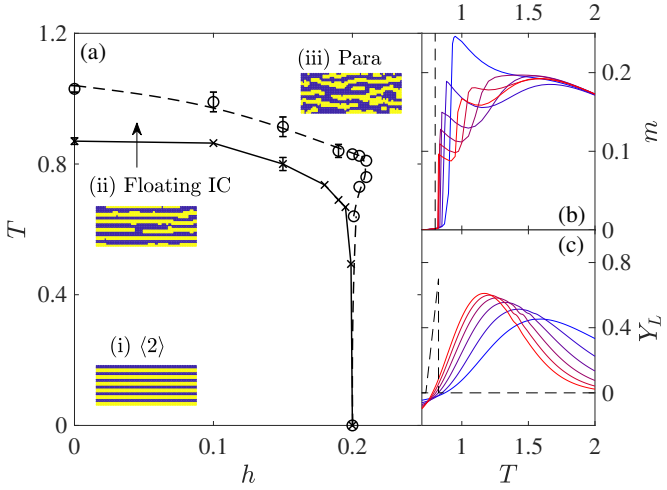

FIG. 4. (a) Phase diagram for the two-dimensional ANNNI model with $\kappa = 0.6$ and varying h. Crosses denote the transition between the antiphase $\langle 2\rangle$ and the floating IC phase, and circles that between the floating IC phase and the paramagnetic phase. Snapshots are obtained as in Fig. 3. (b) Evolution of the magnetization per spin with temperature for $h = 0.15$ obtained from $_\perp$TM with $L = 12 \ldots 32$, from blue to red. Note the clear jump in magnetization at T_{c2} (dashed line). (c) Y_L for $h = 0.205$ obtained from $_\parallel$TM with $L = 5 \ldots 15$, from blue to red. Extrapolating characteristic temperatures (as in Fig. 2) shows that the floating IC phase emerges at intermediate T as $Y_L > 0$ (dashed line).

and 1.27[30]. (Earlier theoretical estimates vary even more, from $T_{c1} \approx T_{c2}$[26,32] to 1.64[23].) Because finite-size corrections and equilibration difficulties in simulating this regime are notoriously pronounced, such discrepancy is not particularly surprising. The good agreement between multiple characteristic temperatures and the small curvature of the fits (suggestive of a relatively small preasymptotic correction) tend instead to support our estimate. As a further test of the scenario $T_{high} = T_{c1} = T_{c2}$, we note that the extrapolated $T_{high}(L \to \infty|\kappa = 0.6)$ reaches a minimum of 1.00 for $t = 0.75$, still well above T_{c2}. Interestingly, the DMRG study that supports this scenario[26] was conducted with $_\perp$TM. A DMRG formalism with $_\parallel$TM may also locate T_{c1} differently and more robustly, although the confounding effect of other approximations cannot be excluded. In any event, results of our exact transfer matrix treatment as well as recent extensive simulations[14] strongly support $T_{c1} > T_{c2}$.

The distinctiveness of the two characteristic temperatures suggests that θ monotonically increases with T for a fixed κ in the floating IC phase. Extrapolating Y_L at different characteristic temperatures, namely $Y_{L,max}$, $Y_{L,high}$ and $Y_{L,min}$, $Y_{L,mid}$ (as in Fig. 2(f)), provides approximations for $\theta(T_{c1};\kappa)$ and $\theta(T_{c2};\kappa)$, respectively. These exponents vary remarkably little with κ (Fig. 3 (inset)). The two distinct transition temperatures thus likely persist as κ increases, even though a quantitative distinction between the two transition temperatures by finite-size scaling is here only feasible up to $\kappa \approx 2$. The non-monotonic behavior of Y_L that gives rise to this behavior in the thermodynamic limit hence lends support to the floating IC phase surviving as $\kappa \to \infty$, and goes against the finite-κ Lifshitz point scenario.[18,51]

For κ slightly smaller than 1/2, a distinct feature emerges in Y_L. For example, for $\kappa = 0.49$ a narrow disordered region with $Y_L \to 0$ is squeezed between the ferromagnetic phase and the floating IC phase (Fig. 2(b)). For $\kappa < 1/2$, a disorder line subdivides the disordered regime,[25,52] where the correlation length exhibits a kinked local minimum. Given that the disorder line identified by the fixed point of Z_L (Fig. 2(d)) extends down to the multiphase point at (κ=1/2,T=0),[23,53] we conclude that the floating IC and Ising ferromagnetic phases never meet for $T > 0$. This analysis thus confirms the reentrance of the floating IC phase in this regime, as various theoretical treatments have proposed.[23,24] The disorder line for decreasing $\kappa < 1/2$ is also found to be asymptotically tangent to $\kappa = 0$ as $T \to \infty$, instead of $\kappa = 0.25$, as was previously suggested.[23] Combining these various observations provides a complete quantitative phase diagram for the two-dimensional ANNNI model at $h = 0$ (Fig. 3).

Phases diagram for $h > 0$. As noted above, the ANNNI model in lattice-gas representation can be viewed as a

minimal model for lamellar microphases. For this model, as in generic SALR microphase formers,[2] at low T and small κ a coexistence regime around $h = 0$ separates the condensed (-1 spins dominated) and gas ($+1$ spins dominated) phases, while for $\kappa > 1/2$ lamellar microphases replace macroscopic phase separation. Increasing h then depresses the $\langle 2 \rangle$ melting temperature down to $T \to 0$ at $h^* = 2\kappa - 1$.[54] Figure 4 presents results for $\kappa = 0.6$ (for which $h^* = 0.2$). At large h the ground state is a saturated paramagnetic phase without modulations. Although this regime exhibits spin configurations akin to those of a ferromagnetic phase, its correlation length is finite. At smaller h—as for $h = 0$—a floating IC phase intercalates between the commensurate $\langle 2 \rangle$ and the paramagnetic phases. The ${}_\perp$TM route confirms that the magnetization per spin, m, remains null in the $\langle 2 \rangle$ phase and jumps (as does u) at the transition (Fig. 4(b)). By contrast, spin layers preferentially align with the external field in the floating IC phase, which leads to the magnetization increasing stepwise with temperature. At yet higher temperatures, in the paramagnetic phase m again decreases as entropy increasingly dominate. Slightly above h^* the floating IC phase reenters, in a way reminiscent of the $J_1 - J_2$ model.[55] The behavior of the local exponent Y_L, which crosses at the lower-T boundary of the IC phase and peaks at the higher-T phase boundary (Fig. 4(c)), is also similar to the reentrance in Fig. 2(b). Extrapolating these special temperatures gives the phase boundaries in Fig. 4(a). Note that for $h \gtrsim 0.22$, the order of the extrapolated lower and higher temperature boundary of the IC phase changes and $Y_L(T_{c1})$ is projected to vanish. The thermodynamic floating IC phase then terminates, even though strong finite-size echoes of it appear to persist.

Conclusion. Using a numerical TM approach, we have resolved various ambiguities in the phase diagram of the two-dimensional ANNNI model both with and without an external field. Our results confirm the reentrance scenario for the floating IC phase, suggest that the floating IC phase persists up to $\kappa \to \infty$, and that the exponent of algebraic divergence of the correlation length remains robust. Although larger-scale studies could bring further credence to these findings, the latter two motivate additional theoretical studies regardless. Because the accuracy of the TM approach clearly outperforms that of prior finite-size simulations, we also expect that methodological improvements in that latter field will be sought out. Finally, our results motivate considering the TM approach for resolving the equilibrium phase behavior of related frustrated models, such as the BNNNI[56] and lattice surfactant[57–59] models. The range of system sizes now accessible further suggest that extending the TM formalism to three-dimensional models[60] might nearly be within computational reach.

ACKNOWLEDGMENTS

We acknowledge support from the Simons Foundation (#454937) and from the National Science Foundation Grant No. DMR-1749374. The computations were carried out on the Duke Compute Cluster. Data relevant to this work have been archived and can be accessed at the Duke Digital Repository.[61]

* patrick.charbonneau@duke.edu

[1] F. Sciortino, S. Mossa, E. Zaccarelli, and P. Tartaglia, Phys. Rev. Lett. **93**, 055701 (2004).
[2] A. Ciach, J. Pękalski, and W. T. Góźdź, Soft Matter **9**, 6301 (2013).
[3] Y. Zhuang and P. Charbonneau, J. Phys. Chem. B **120**, 7775 (2016).
[4] C. P. Royall, Soft Matter **14**, 4020 (2018).
[5] M. Seul and D. Andelman, Science **267**, 476 (1995).
[6] O. Portmann, A. Vaterlaus, and D. Pescia, Nature **422**, 701 (2003).
[7] F. Hassler and D. Schuricht, New J. Phys. **14**, 125018 (2012).
[8] M. Caffrey, Annu. Rev. Biophys. **38**, 29 (2009).
[9] L. Fink, A. Steiner, O. Szekely, P. Szekely, and U. Raviv, Langmuir **35**, 9694 (2019).
[10] T. Lecuit and P.-F. Lenne, Nat. Rev. Mol. Cell Biol. **8**, 633 (2007).
[11] C.-P. Heisenberg and Y. Bellaïche, Cell **153**, 948 (2013).
[12] M. Henkel, M. Pleimling, C. Godreche, and J.-M. Luck, Phys. Rev. Lett. **87**, 265701 (2001).
[13] K. Zhang and P. Charbonneau, Phys. Rev. Lett. **104**, 195703 (2010).
[14] T. Shirakura, F. Matsubara, and N. Suzuki, Phys. Rev. B **90**, 144410 (2014).
[15] Y. Zhuang, K. Zhang, and P. Charbonneau, Phys. Rev. Lett. **116**, 098301 (2016).
[16] Z. Lei, W. Krauth, and A. C. Maggs, Phys. Rev. E **99**, 043301 (2019).
[17] M. E. Fisher and W. Selke, Phys. Rev. Lett. **44**, 1502 (1980).
[18] W. Selke, Z. Phys. B: Condens. Matter **43**, 335 (1981).
[19] M. Beccaria, M. Campostrini, and A. Feo, Phys. Rev. B **73**, 052402 (2006).
[20] M. Beccaria, M. Campostrini, and A. Feo, Phys. Rev. B **76**, 094410 (2007).
[21] J. Villain and P. Bak, J. Phys. (Paris) **42**, 657 (1981).
[22] J. Oitmaa, J. Phys. A **18**, 365 (1985).
[23] A. Finel and D. de Fontaine, J. Stat. Phys. **43**, 645 (1986).
[24] M. A. S. Saqi and D. S. McKenzie, J. Phys. A **20**, 471 (1987).
[25] W. Selke, Phys. Rep. **170**, 213 (1988).
[26] R. Derian, A. Gendiar, and T. Nishino, J. Phys. Soc. Jpn. **75**, 114001 (2006).
[27] W. Selke and M. E. Fisher, Z. Phys. B: Condens. Matter **40**, 71 (1980).
[28] J. M. Kosterlitz and D. J. Thouless, J. Phys. C **6**, 1181 (1973).
[29] A. Sato and F. Matsubara, Phys. Rev. B **60**, 10316 (1999).
[30] E. Rastelli, S. Regina, and A. Tassi, Phys. Rev. B **81**,

094425 (2010).
[31] F. Matsubara, T. Shirakura, and N. Suzuki, Phys. Rev. B **95**, 174409 (2017).
[32] T. Shirahata and T. Nakamura, Phys. Rev. B **65**, 024402 (2001).
[33] A. K. Chandra and S. Dasgupta, J. Phys. A **40**, 6251 (2007).
[34] W. Pesch and J. Kroemer, Z. Phys. B: Condens. Matter **59**, 317 (1985).
[35] P. D. Beale, P. M. Duxbury, and J. Yeomans, Phys. Rev. B **31**, 7166 (1985).
[36] R. B. Lehoucq, D. C. Sorensen, and C. Yang, *ARPACK users' guide: solution of large-scale eigenvalue problems with implicitly restarted Arnoldi methods* (SIAM, 1998).
[37] Y. Hu and P. Charbonneau, Soft Matter **14**, 4101 (2018).
[38] M. J. Godfrey and M. A. Moore, Phys. Rev. E **91**, 022120 (2015).
[39] J. F. Robinson, M. J. Godfrey, and M. A. Moore, Phys. Rev. E **93**, 032101 (2016).
[40] Y. Hu, L. Fu, and P. Charbonneau, Mol. Phys. **116**, 3345 (2018).
[41] S. Jin, A. Sen, W. Guo, and A. W. Sandvik, Phys. Rev. B **87**, 144406 (2013).
[42] Y. Hu and P. Charbonneau, arXiv preprint (2020), arXiv:2009.11194.
[43] Y. Qiu, "Spectralib (sparse eigenvalue computation toolkit as a redesigned ARPACK[36])," (2020).
[44] A. E. Ferdinand and M. E. Fisher, Phys. Rev. **185**, 832 (1969).
[45] J. Salas, J. Phys. A **34**, 1311 (2001).
[46] P. Nightingale, J. Appl. Phys. **53**, 7927 (1982).
[47] D. Landau and K. Binder, Phys. Rev. B **31**, 5946 (1985).
[48] V. L. Pokrovsky and A. L. Talapov, Phys. Rev. Lett. **42**, 65 (1979).
[49] B. Nienhuis, H. J. Hilhorst, and H. W. J. Blote, J. Phys. A **17**, 3559 (1984).
[50] P. M. Duxbury, J. Yeomans, and P. D. Beale, J. Phys. A **17**, L179 (1984).
[51] M. N. Barber and P. M. Duxbury, J. Phys. A **14**, L251 (1981).
[52] J. Stephenson, Can. J. Phys. **48**, 1724 (1970).
[53] I. Peschel and V. J. Emery, Z. Phys. B: Condens. Matter **43**, 241 (1981).
[54] P. Rujan, W. Selke, and G. V. Uimin, Z. Phys. B: Condens. Matter **53**, 221 (1983).
[55] A. I. Guerrero, D. A. Stariolo, and N. G. Almarza, Phys. Rev. E **91**, 052123 (2015).
[56] J. Oitmaa, M. T. Batchelor, and M. N. Barber, J. Phys. A **20**, 1507 (1987).
[57] J. C. Wheeler and B. Widom, J. Am. Chem. Soc. **90**, 3064 (1968).
[58] B. Widom, J. Chem. Phys. **84**, 6943 (1986).
[59] N. G. Almarza, J. Pękalski, and A. Ciach, J. Chem. Phys. **140**, 164708 (2014).
[60] H. L. Richards, M. A. Novotny, and P. A. Rikvold, Phys. Rev. B **48**, 14584 (1993).
[61] "Duke digital repository," https://doi.org/10.7924/xxxxxxxxx.